Improved Stability of a C-C Bond Coupling Catalyst for Conversion of CO_2 to Acetate

Undergraduate Research Thesis

Presented in partial fulfillment of the requirements for graduation *with honors research distinction* in Chemistry in the undergraduate colleges of The Ohio State University

by

Skyler Ware

The Ohio State University

April 2018

Project Advisor: Professor L. Robert Baker, Department of Chemistry

Abstract

The electrochemical conversion of carbon dioxide to value-added, multi-carbon products has been studied as a pathway to renewable fuel sources and as an alternative to current carbon capture and storage methods. Delafossite copper iron oxide films have been shown to thermally fixate carbon dioxide and selectively catalyze carbon-carbon bond coupling from CO_2 to produce acetate. However, the catalyst alone is not stable and deactivates after approximately ten minutes following the reductive dissolution of surface iron species. The addition of gaseous oxygen as a sacrificial electron acceptor prevents the reductive dissolution of iron and stabilizes the catalyst for several hours; however, excess oxygen scavenges the electrons used for acetate production, resulting in lower yield and reduced conversion efficiency. The purpose of this study was to examine the effects of oxygen at various flow rates on catalyst stability and on acetate formation, as well as to determine the sources of carbon and hydrogen in the final product. The electrolyte solution was purged with both carbon dioxide and oxygen before and during electrolysis using the copper iron oxide catalyst as the working electrode. The optimal oxygen flow rate significantly slowed iron reduction and stabilized the catalyst for up to 12 hours with only a modest drop in acetate selectivity. This enhanced stability allowed further characterization of the carbon source as thermally fixed ambient CO_2, which occurs during annealing of the catalyst. Future studies will further examine the surface chemistry over long-term reductions, including the full mechanism of acetate production and the role of both metals and their oxidation states in the catalytic process.

I. Introduction

Rising levels of atmospheric carbon dioxide present one of the greatest threats to the environment. As of 2016, atmospheric CO_2 levels have risen above 400ppm, an increase of over 100ppm since pre-industrial times[1]. Though CO_2 levels in the atmosphere vary over time, an analysis of long-term trends shows a sharp increase in CO_2 levels over the past 150 years that can only be attributed to anthropogenic activity. Figure 1 shows this increase[2], which began around the time of the industrial revolution.

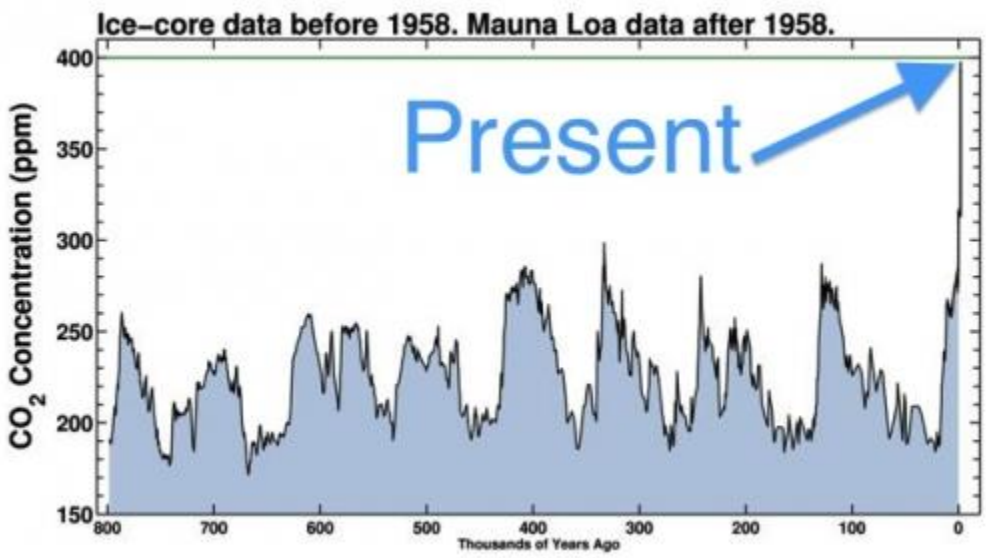

Figure 1. Atmospheric carbon dioxide concentration, 800,000 years b.p. to present.

One of the major challenges facing researchers today is closing the carbon cycle[3,4] and recycling or reusing some of this excess carbon. CO_2 itself is rarely useful in industrial settings, but it can serve as a useful feedstock for generating other carbon-containing species[5-10]. Most of these species have been C1 products, i.e. compounds that only contain one carbon atom, such as formate or carbon monoxide. Carbon-carbon bond coupling to form >C2 species can rarely be

accomplished without high overpotentials or rare earth catalysts. The most common catalysts for C-C bond coupling are ruthenium[11-13], iridium[14-17], and rhodium[17,18], which cost $100-$1,000 per ounce[19]. Copper is one of the only low-cost, earth-abundant metals to catalyze C-C bond coupling.

Several mechanisms have been proposed for the reduction of CO_2 to multicarbon products, but none have been explicitly verified. Centi and coworkers[20] suggest a mechanism that proceeds through an adsorbed carboxylate intermediate (Figure 2) to produce acetate and methanol. However, no intermediates in the reduction of CO_2 have been isolated or spectroscopically identified. Determination of the specific electrochemically active site for a given catalyst and a thorough understanding of the CO_2 reduction mechanism will promote the design of more efficient catalysts for C-C bond coupling.

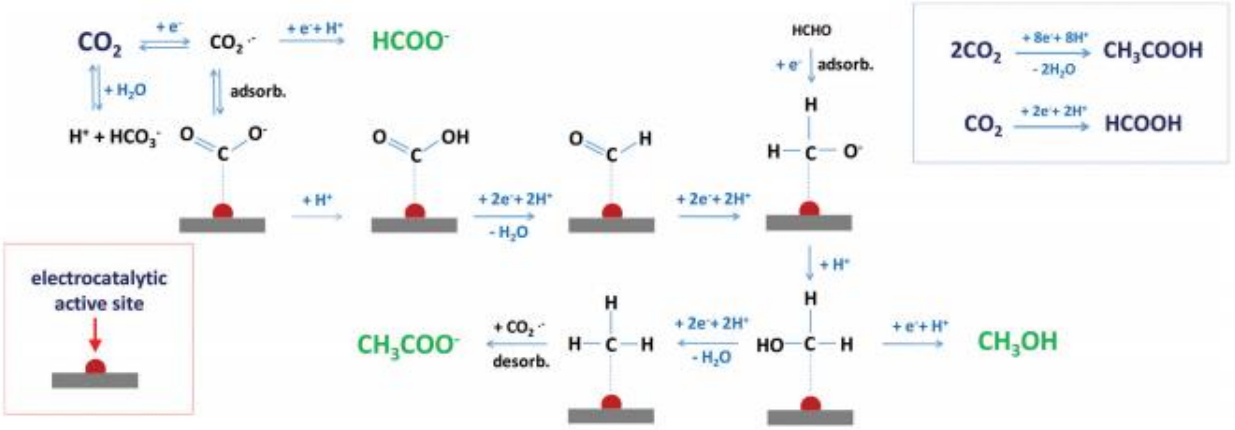

Figure 2. Proposed mechanism for reduction of carbon dioxide to formate, acetate, and methanol.

In 2017, the Baker group developed a mixed copper iron oxide catalyst that selectively reduces CO_2 to acetate at up to 80% Faradaic efficiency[21]. Figure 3 shows SEM/EDX images of the

catalyst, indicating its structure and even distribution of surface copper and iron. This catalyst consists of inexpensive materials and can be produced with minimal energy input, but it deactivates within ten minutes under the electrochemical conditions required to produce acetate. Previous studies have shown that this deactivation follows the reductive dissolution of surface iron species[21] – Fe(III) is more stable in the crystal lattice than Fe(II), and the Fe(II) species eventually dissolves if it is not reoxidized. In order for $CuFeO_2$ to be a viable industrial catalyst for CO_2 reduction to acetate or other multicarbon products, the catalyst must be stabilized. The addition of gaseous oxygen as an electron acceptor during electrolysis prevents iron reduction and stabilizes the catalyst for several hours; however, excess oxygen also scavenges electrons used for acetate production. This work describes the effects of oxygen at various flow rates on catalyst stability and acetate formation as well as progress toward elucidating the mechanism of CO_2 reduction.

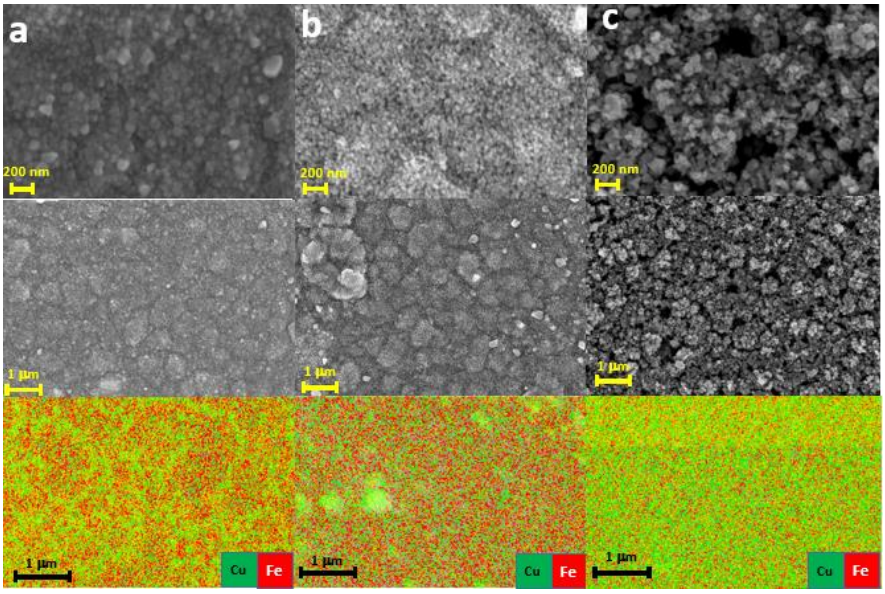

Figure 3. SEM and EDX images of the copper iron oxide catalyst (a) as prepared, (b) post electrolysis under CO_2 and O_2 purging, and (c) post electrolysis under CO_2 saturated conditions.

II. Materials and Methods

Materials

Unless otherwise stated, all reagents were purchased from Sigma Aldrich and used without further purification. Fluorine-doped tin oxide (FTO) glass substrates were purchased from Sigma Aldrich. Carbon dioxide (99.9% purity) and oxygen (99.993% purity) gas cylinders were purchased from Praxair. Ag/AgCl (4M NaCl) reference electrode was purchased from BASi. All glassware used in electrode preparation, deposition, and electrolysis was oven-dried at 85°C.

Electrode Preparation

All catalysts were prepared by electrodeposition in a custom single compartment cell using a Ag/AgCl reference electrode. Thin-film platinum counter electrodes were prepared by sputtering 20nm of titanium and 100nm of platinum onto a glass slide. Before deposition, FTO glass was immersed in methanol and sonicated for 5 minutes to clean the conductive surface. The methanol was removed and the substrate was rinsed 8 times with DI water and dried with nitrogen. The temperature during electrodeposition was controlled using a silicone oil bath.

Catalyst Deposition

$CuFeO_2$ films were electrodeposited from a solution of 1mM $Cu(NO_3)_2{\cdot}xH_2O$, 3mM $Fe(ClO_4)_3{\cdot}xH_2O$, and 100mM $KClO_4$ in anhydrous dimethyl sulfoxide (DMSO). The plating solution was sonicated for 5 minutes in a sealed container to fully dissolve the copper and iron salts. Deposition was performed on FTO glass substrates measuring 3.5x3.5cm for 45 minutes using 50mL plating solution (for time dependent experiments) or on substrates measuring

1.9x1.9cm for 30 minutes using 25mL plating solution (for O_2 flow rate dependent experiments and carbon source determination). The deposition was performed at 83°C at an applied potential of -0.3V vs Ag/AgCl. Samples were annealed for 3.5 hours following deposition in either a custom designed batch mode gas-phase reactor connected to a gas manifold and a boron nitride substrate heater (carbon source experiments) or an annealing furnace in ambient atmosphere (all other experiments).

Catalyst Characterization

$CuFeO_2$ electrode surfaces were characterized by X-ray photoelectron spectroscopy (Kratos Axis Ultra). A monochromatic Al Kα source (hν = 1,486.6 eV) was operated at 120W with a 12kV accelerating voltage. The ion-pumped chamber generated a base pressure of $1.6x10^{-9}$ mbar. Surface atomic fractions were determined by peak area fitting using CasaXPS software.

SEM images and elemental mapping by energy dispersive x-ray spectroscopy (EDX) were obtained using a Carl Zeiss Ultra 55 Plus field-emission SEM.

Electrochemical Measurements

All electrochemical experiments were performed using a Biologic SP-50 potentiostat and a three-electrode system consisting of a Ag/AgCl reference electrode, a platinum counter electrode, and the as-prepared catalyst as the working electrode.

Carbon source determination and O_2 flow rate dependent experiments were performed in a custom designed dual compartment poly(etherethylketone) (PEEK) reactor. One compartment contained a platinum mesh counter electrode, and the other contained the Ag/AgCl reference

electrode. The two compartments, separated by a Nafion membrane, were clamped together, and the working electrode was clamped against an O-ring on the front face of the PEEK reactor to create a closed cell with 4mL volume on the working electrode side of the membrane.

Time dependent experiments were performed in a custom designed dual compartment 17mL glass H-cell. The compartments were separated by a Nafion membrane, with one compartment containing a thin-film platinum counter electrode and the other containing the Ag/AgCl reference electrode and the as-prepared working electrode.

The Nafion membrane was prepared according to the procedure outlined by Meng and coworkers.[22] The cell was filled with 0.1M aqueous $NaHCO_3$ electrolyte, and carbon dioxide and oxygen were purged simultaneously into the working electrode compartment of the cell for two hours before beginning electrolysis. Gas flow rates were controlled using flow meters purchased from McMaster-Carr.

Cyclic voltammograms were collected in a custom single compartment cell using a Ag/AgCl reference electrode and a thin-film platinum counter electrode. All potentials were then standardized to the reversible hydrogen electrode (RHE) using the Nernst equation

$$E_{RHE} = E_{Ag/AgCl} + 0.059pH + E^0_{Ag/AgCl}$$

where E_{RHE} is the calculated potential versus RHE, $E_{Ag/AgCl}$ is the measured potential versus the Ag/AgCl reference electrode, and $E^0_{Ag/AgCl}$ is the standard potential of the Ag/AgCl reference electrode (0.197V).

Product Detection

^{1}H-NMR (400MHz DPX) was collected from a solution of the post-reaction electrolyte and D_2O in an 8:1 ratio. Acetonitrile was used as an internal standard.

III. Results and Discussion

Stability of the $CuFeO_2$ Catalyst

Figure 4 shows the improved stability of the $CuFeO_2$ catalyst under oxygen-saturated conditions. When the electrolyte is purged with CO_2 only, the current decays to zero after approximately ten minutes. This indicates that the flow of electrons has stopped, so the catalyst no longer produces acetate. At the same time, the iron reductively dissolves from the catalyst surface. Figure 5 shows x-ray photoelectron spectra of catalysts after electrolysis under various oxygen flow rates. In the copper spectrum, the features at 930 and 951 eV indicate the presence of Cu(I) and the peaks at 942 eV and 963 eV are satellite features indicating the presence of Cu(II) species. At 0 standard cubic centimeters per minute (sccm) oxygen (CO_2-saturated conditions), all of the surface copper is reduced to Cu(I) and the iron has leached from the catalyst surface. The addition of a small amount of oxygen (40 sccm) stabilizes the copper in the Cu(II) state, but the iron still leaches. As the oxygen flow rate is increased, less iron leaches until at 360 sccm oxygen, the post-reaction catalyst shows the same composition as the fresh, unreacted catalyst. As shown in Figure 4, the current under these oxygen-saturated conditions remains stable for over two hours.

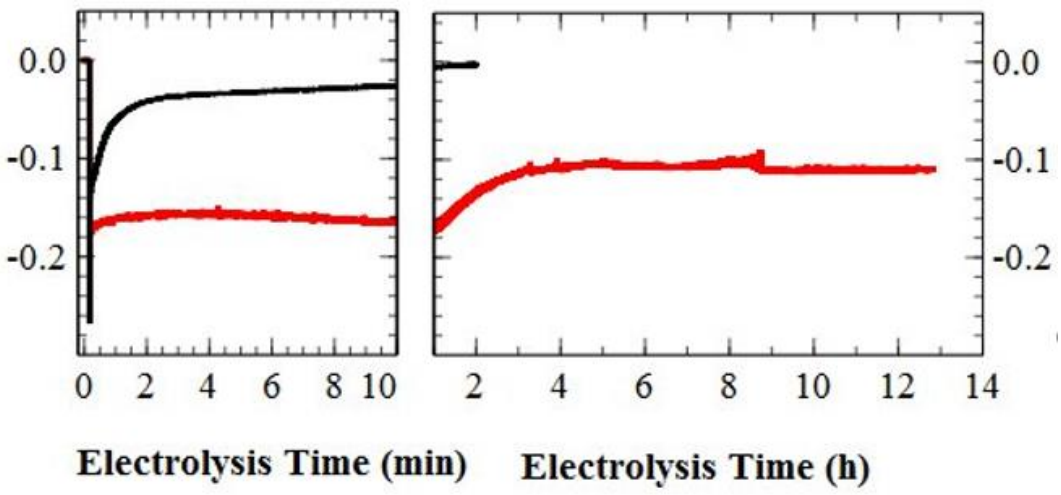

Figure 4. Current profile of the copper iron oxide electrode during the 2 hours of electrolysis in CO_2 saturated (black) and CO_2/O_2 saturated (red) bicarbonate electrolyte (0.1 M) under −0.4 V vs.Ag/AgCl bias.

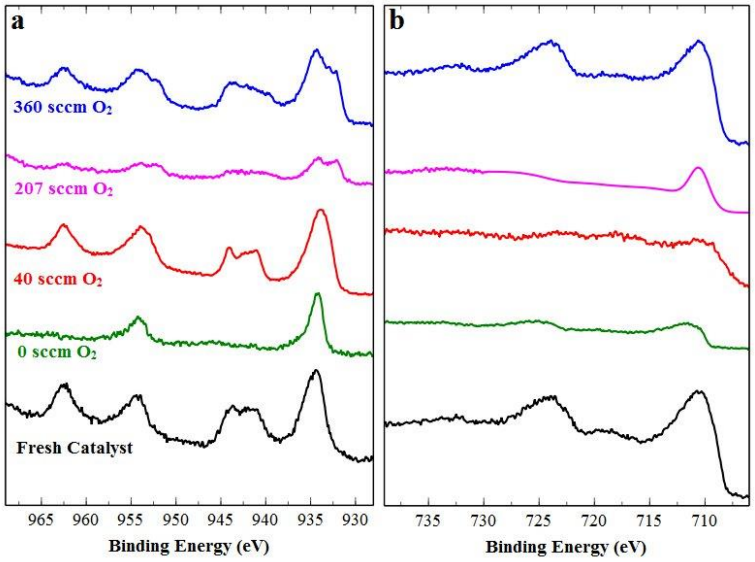

Figure 5. XPS spectra of Cu 2p (a) and Fe 2p (b) in the copper iron oxide catalyst under variable oxygen flow rate.

Cyclic voltammograms of the catalyst further support the conclusion that the surface iron species is stabilized upon addition of gaseous oxygen. Figure 6 shows CV curves of the catalyst under various gas purging conditions. Table 1 shows the pH of each of the electrolytes after 30 minutes of purging; these values were used to standardize the potential measurements to the reversible hydrogen electrode. The reduction feature at 0.35V vs RHE is attributed to a combination of Fe(III) → Fe(II) and CO_2 reduction, and the corresponding reoxidation feature at 0.75V is attributed to Fe(II) → Fe(III). In the argon-saturated and CO_2-saturated cases, much of the surface iron is reduced and subsequently reoxidized, but when oxygen is added to the CO_2-saturated conditions, the reoxidation feature disappears and the reduction peak decreases in area. Here, we attribute this to the oxygen stabilizing the iron against reduction by scavenging excess electrons. The remaining area in the reduction feature can be attributed to irreversible CO_2 reduction. Furthermore, in the oxygen-saturated case, the reduction feature is shifted to less positive bias and the reoxidation feature disappears entirely. In this case, we attribute the reduction feature to irreversible oxygen reduction, and the absence of the iron reoxidation feature suggests that the iron is fully stabilized in the oxidized Fe(III) state.

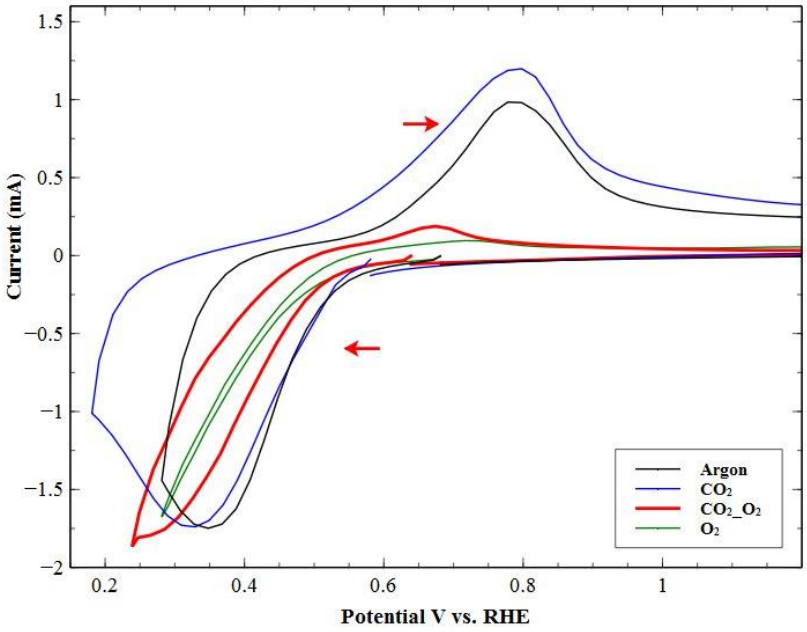

Figure 6. Cyclic voltammograms of the copper iron oxide electrode in CO_2 saturated (blue), argon saturated (black), CO_2/O_2 saturated (red), and O_2 saturated (green) 0.1 M $NaHCO_3$ electrolyte solution (scan rate: 50 mV/s). Arrows indicate direction of scan.

Purge Gas	**pH**
Unpurged electrolyte	8.32
Ar	9.00
CO2	6.75
CO2/O2	7.48
O2	9.05

Table 1: pH of 0.1M bicarbonate electrolyte under various purging conditions.

Because oxygen acts as an electron scavenger to prevent the iron in the catalyst from being reduced, we expected that excess oxygen would scavenge electrons used to produce acetate and that the acetate yield would thus significantly decrease. On the contrary, the addition of

gaseous oxygen seems to promote acetate formation. Figure 7 shows acetate yield (black) and Faradaic efficiency (red) as a function of oxygen flow rate. As the oxygen flow rate increases, both the acetate yield and Faradaic efficiency increase, reaching a maximum value at 360 sccm oxygen. At oxygen flow rates above 360 sccm (not shown), both the acetate yield and Faradaic efficiency decrease. Since the surface iron remains stable in its oxidized state as shown by XPS, we attribute this to competing kinetics between acetate formation and oxygen reduction to a hydroxyl species.

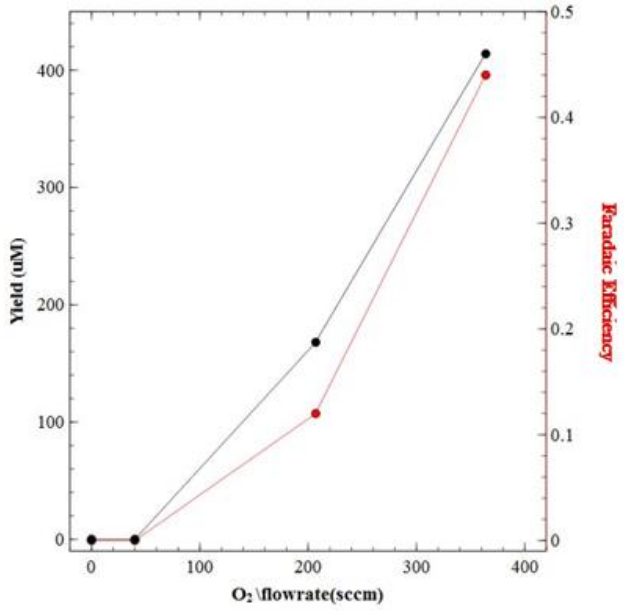

Figure 7. Acetate yield (black) and Faradaic efficiency (red) as a function of oxygen purge rate.

Time dependent electrolysis shows that the catalyst is stable and produces acetate for up to twelve hours (Figure 8). ^{1}H-NMR data were collected and used to calculate the Faradaic efficiency of acetate production every hour for a 24-hour period. The acetate yield steadily increased for the first twelve hours, after which the yield ceased increasing and the Faradaic efficiency monotonically decreased. Time dependent XPS data (Figure 9) show that this

deactivation may be partially related to the loss of surface iron species after extended electrolysis times. After 8 hours, the iron is still stable, but after 32 hours, the surface iron has leached. As shown below, the total acetate yield may also be limited by the amount of adsorbed CO_2 on the catalyst surface.

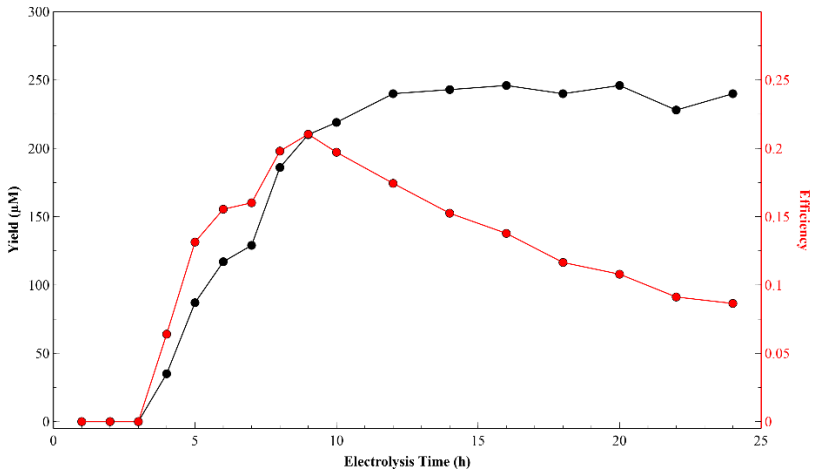

Figure 8. Time-profiled acetate yield (black) and Faradaic efficiency (red) with the copper iron oxide catalyst under CO_2 and O_2 purging in 0.1M bicarbonate electrolyte.

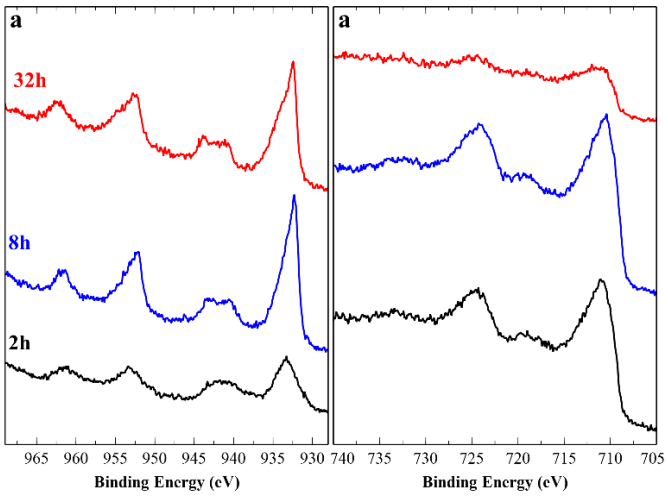

Figure 9: Time profiled XPS of the copper iron oxide catalyst under CO_2 and O_2 purging in 0.1M bicarbonate electrolyte.

Carbon and Hydrogen Sources

The electrolysis reaction described above is conducted in the absence of light at -0.4V vs Ag/AgCl. At pH 7.48 (CO_2 and O_2 purging, see Table 1), this corresponds to a potential of 0.238V vs RHE. The standard reduction potential of CO_2 to acetate is 0.290V vs RHE[23]; therefore, this reaction occurs at roughly 0.05V underpotential. This finding suggests that CO_2 gas purged into the electrolyte during electrolysis may not be the source of both carbons in the acetate product and motivates a second study to verify the sources of carbon and hydrogen in the detected acetate.

To explicitly determine the carbon and hydrogen sources in the acetate product, we ran a series of experiments systematically eliminating possible carbon donors. Table 2 shows several experiments leading to the assignment of the carbon source. The first row lists the conditions for a standard CO_2 reduction experiment to produce acetate. Highlighted sections in the table signify deviations from that standard experiment, testing or eliminating the possibility of a given carbon source.

The second and third rows in Table 2 describe attempts to rule out DMSO from the plating solution as the carbon source. To test this, the $CuFeO_2$ catalyst was electrodeposited in an aqueous solution, but no annealing or electrolysis conditions were changed. Without DMSO present during deposition, the catalyst still produced 305µM acetate during electrolysis. Another $CuFeO_2$ catalyst was electrodeposited in d^6-DMSO. If this DMSO was the source of the methyl group in acetate, the proton signature would not be visible in ^{1}H-NMR since deuterium has zero nuclear magnetic moment. However, this catalyst produced similar acetate yields

detectable by proton NMR. From these two experiments, we conclude that DMSO is not the source of either carbon in the acetate product.

The fourth row in table 2 shows attempts to determine whether either carbon was donated by the bicarbonate electrolyte in equilibrium with dissolved CO_2 from the gas purging lines. We performed the electrolysis in phosphate buffer while purging with oxygen and argon to eliminate any dissolved carbonate species in the electrolyte. This catalyst again produced acetate at high yields, suggesting that the carbon does not come from the electrolyte or from dissolved CO_2.

We next investigated the possibility that thermally adsorbed atmospheric CO_2 captured during annealing was the carbon source. A series of catalysts annealed in air at different temperatures (Table 2, rows 8-10) show that acetate yield increases with annealing temperature, and thus presumably more CO_2 is thermally fixed at higher temperatures. Higher temperatures have not been investigated due to the low stability of the FTO glass substrate above 700°C[24].

Experiment	Plating solution	Annealing atmosphere	Annealing temperature	Electrolyte	Purge gas	Acetate yield
Standard	DMSO	ambient	650°C	0.1M bicarb	CO_2/O_2	
Carbon Source	H_2O	ambient	650°C	0.1M bicarb	CO_2/O_2	305µM
	d^6 DMSO	ambient	650°C	0.1M bicarb	CO_2/O_2	280µM
	DMSO	ambient	650°C	0.1M phosphate	O_2/argon	350µM
	DMSO	O_2/N_2 in reactor	400°C	0.1M bicarb	CO_2/O_2	50µM
	DMSO	$O_2/N_2/CO_2$ in reactor	400°C	0.1M bicarb	CO_2/O_2	200µM
Temperature Dependence	DMSO	ambient	unannealed	0.1M bicarb	CO_2/O_2	<LOD
	DMSO	ambient	300°C	0.1M bicarb	CO_2/O_2	50µM
	DMSO	ambient	650°C	0.1M bicarb	CO_2/O_2	155µM

Table 2. Determination of the carbon source in the acetate product. Highlighted sections indicate deviations from the standard CO_2 reduction experiment.

We additionally annealed two catalysts in a custom designed gas phase reactor under controlled atmosphere (rows 6 and 7 in Table 2). The first catalyst, annealed in an atmosphere of nitrogen and oxygen roughly mimicking ambient atmosphere, produced very little acetate. However, the second catalyst was annealed under similar conditions but with 1 torr CO_2 added to the atmosphere. This catalyst produced significantly higher yields, comparable to those of catalysts annealed under ambient atmosphere. These two experiments suggest that thermally adsorbed ambient CO_2 is the source of both carbons in the acetate product. Experiments to confirm this with $^{13}CO_2$ are under way, as well as experiments to determine if the catalyst can be regenerated by adsorbing additional CO_2 during a second round of annealing and electrolysis.

Table 3 shows attempts to elucidate the proton source on the methyl group. DMSO from the plating solution was already ruled out as the proton donor (see above). We next tested the possibility that the electrolyte, either bicarbonate or phosphate, was the proton donor by conducting electrolysis in an aprotic electrolyte, $KClO_4$. This produced slightly lower but still significant acetate yields. We achieved similar yields by repeating the above experiment using $KClO_4$ prepared in D_2O to eliminate the possibility that water from the electrolyte solution was the proton source. These experiments suggest that ambient adsorbed water may be the proton source since changes to the electrolyte do not eliminate the acetate product as detected by ^{1}H-NMR. However, these experiments are not yet conclusive. D_2O will undergo proton exchange with ambient water if left exposed to air, and there may be pH effects from using neutral salts in the electrolyte rather than those derived from weak acids. Further experiments, such as

preparing the catalyst and running electrolysis in a tightly controlled environment such as a glovebox, are required to conclusively determine the proton source.

Electrolyte	**Plating solution**	**Acetate Yield**
0.1 M $NaHCO_3$	d^6-DMSO	280 uM
0.1 M $KClO_4$ in H_2O	DMSO	100 uM
0.1M $KClO_4$ in D_2O	DMSO	75 uM

Table 3. Determination of the proton source in the acetate product.

Ethanol

Some unannealed catalysts have been shown to produce ethanol during electrolysis. These catalysts were deposited as usual, but rather than being stored in ambient air for several hours before electrolysis, they were used in electrolysis immediately after deposition without thermal annealing. The exact nature of this mechanism is unknown, but the product distribution may be influenced by different oxidation states of the metals in the catalyst. The carbon species on the catalyst surface appear to be the same for unannealed and annealed catalysts as shown by XPS in Figure 10. The peaks at 284.8 eV represent adventitious carbon, the peaks at 289 eV represent metal carbonates, and the features at 293 and 296 eV correspond to potassium and are likely present from the $KClO_4$ electrolyte used in deposition. However, the surface copper in the unannealed catalyst is almost exclusively present as Cu(I), while in the annealed catalyst the surface copper is split between Cu(I) and Cu(II), as shown in Figure 11. The features at 930 and 951 eV indicate the presence of Cu(I), and the features at 940 and 961 eV indicate the presence of Cu(II). The crystal structure of the unannealed catalyst has not been defined and is

likely different from the delafossite structure of the annealed $CuFeO_2$. Further study is needed to understand the mechanism of ethanol formation and the factors that influence product distribution between ethanol and acetate.

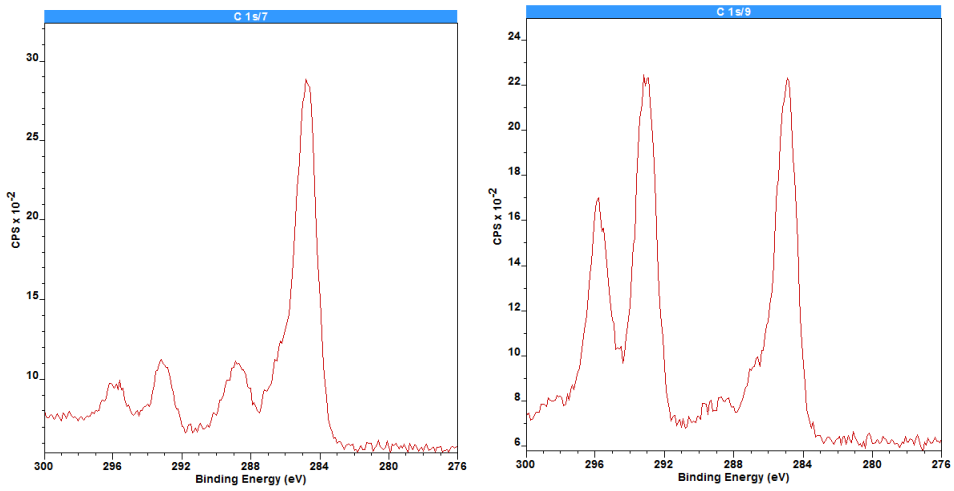

Figure 10. XPS of carbon in unannealed (left) and annealed (right) copper iron oxide catalysts.

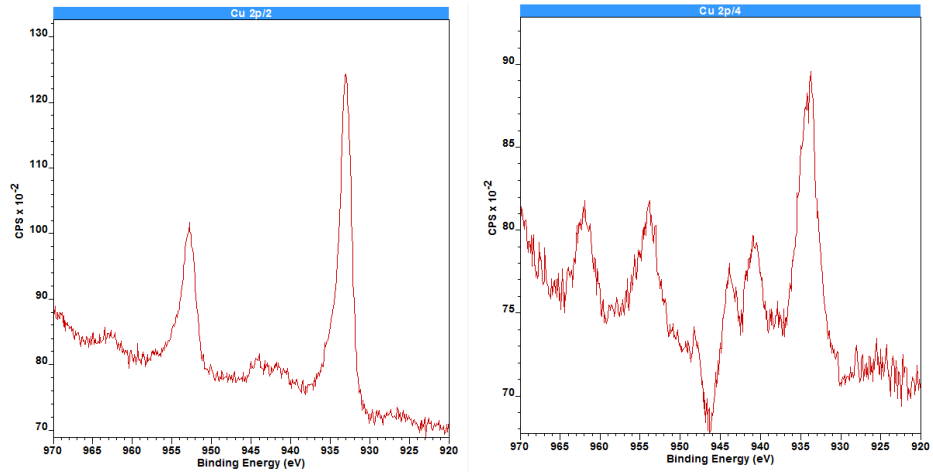

Figure 11. XPS of copper in unannealed (left) and annealed (right) copper iron oxide catalysts.

IV. Conclusions

The addition of gaseous oxygen as an electron acceptor not only stabilizes the surface iron in the $CuFeO_2$ catalyst for several hours, but also promotes acetate formation. The oxygen stabilizes the iron in the form of Fe(III), indicating that this may be the active site for catalysis. This enhanced stability allows for longer-term studies of the mechanism of thermal CO_2 fixation and conversion to multicarbon products for potential use as renewable fuels. By fixing ambient CO_2, this process serves as a safe method of carbon capture and recycling which works toward closing the carbon cycle and reducing the impacts of harmful greenhouse gases.

V. Future Directions

A thorough understanding of the mechanism of acetate formation may influence designs of more efficient catalysts for CO_2 reduction. Future studies will use sum frequency generation to probe the binding modes and sites of carbon species in situ in order to elucidate a detailed understanding of the active sites for catalysis and the CO_2 reduction pathway. Additionally, if ambient CO_2 is confirmed to be the carbon source, then increasing the surface area of the catalyst by depositing on carbon nanotubes or a graphene lattice will likely lead to more binding sites for ambient CO_2 and thus greater yields of multicarbon products. Finally, the possibility of using copper iron oxide or other similar species in tandem catalysis to produce other, more complex products may lead to the formation of better and more efficient fuels.

References

1 Jones, Nicola. "How the World Passed a Carbon Threshold and Why It Matters." Yale University: Yale Environment 360, January 26, 2017.

2 Freedman, Andrew. "The Last Time CO2 Was This High, Humans Didn't Exist." Climate Central: May 3, 2013.

3 Bacastow, R., Keeling, C.D., Woodwell, G.M., and Pecan, E.V. "Atmospheric carbon dioxide and radiocarbon in the natural carbon cycle. II. Changes from A.D. 1700 to 2070 as deduced from a geochemical model." N. p., 1973.

4 Cox, P.M., Betts, R.A., Jones, C.D., Spall, S.A., and Totterdell, I.J. *Nature*, 2000, **408**, 184-187. DOI: 10.1038/35041539

5 Li, C.W. and Kanan, M.W. *J. Am. Chem. Soc*., 2012, **134** (17), pp 7231–7234. DOI: 10.1021/ja3010978

6 Fu, Y., Sun, D., Chen, Y., Huang, R., Ding, Z., Fu, X. and Li, Z. *Angew. Chem*., 2012, **124**: 3420–3423. DOI:10.1002/ange.201108357

7 Dubois, M.R. and Dubois, D.L. *Acc. Chem. Res.*, 2009, **42** (12), pp 1974–1982

8 Chen, Y., Li, C.W., and Kanan, M.W. *J. Am. Chem. Soc*., 2012, **134** (49), pp 19969–19972 DOI: 10.1021/ja309317u

9 Takeda, H., Koike, K., Inoue, H., and Ishitani, O. *J. Am. Chem. Soc.*, 2008, **130** (6), pp 2023–2031. D **OI:** 10.1021/ja077752e

10 Schneider, J., Jia, H., Muckerman, J.T., and Fujita, E. *Chem. Soc. Rev***.**, 2012,**41**, 2036-2051. DOI:10.1039/C1CS15278E

11 Gholamkhass, B., Mametsuka, H., Koike, K., Tanabe, T., Furue, M., and Ishitani, O. *Inorg. Chem.*, 2005, **44** (7), pp 2326–2336. DOI: 10.1021/ic048779r

12 Ishida, H., Tanaka, K., and Tanaka, T. *Organometallics*, 1987, **6** (1), pp 181–186. DOI: 10.1021/om00144a033

13 Sato, S., Morikawa, T., Saeki, S., Kajino, T., and Motohiro, T. *Angew. Chem*., 2010, **49**: 5101-5105. DOI: 10.1002/anie.201000613

14 Schmeier, T.J., Dobereiner, G.E., Crabtree, R.H., and Hazari, N. *J. Am. Chem. Soc*., 2011, **133** (24), pp 9274–9277. DOI: 10.1021/ja2035514

15 Sato, S., Morikawa, T., Kajino, T., and Ishitani, O. *Angew. Chem*., 2013, **125**:1022-1026. DOI: 10.1002/ange.201206137

16 Kang, P., Zhang, S., Meyer, T.J., and Brookhart, M*. Angew. Chem*., 2014, **53**: 8709-8713. DOI: 10.1002/anie.201310722

17 Bolinger, C.M., Story, N., Sullivan, B.P., and Meyer, T.J. *Inorg. Chem*., 1988, **27** (25), pp 4582–4587. DOI: 10.1021/ic00298a016

18 Yoshinori, K., Hironaka, N., Takanori, N., Kiyoshi, I., and Koji, T. *Chem. Lett*., 1994, **23**:2175-2178. DOI: 10.1246/cl.1994.2175

19 https://www.quandl.com/collections/markets/rare-metals

20 Genovese, C., Ampelli, C., Perathoner, S., and Centi, G. *Green Chem*., 2017, **19**, 2406. DOI: 10.1039/c6gc03422e

21 Yang, X., Fugate, E., Mueanngern, Y., and Baker, L.R. *ACS Catalysis*, 2017, **7**, 177-180. DOI: 10.1021/acscatal.6b02984

22 Wang, Y., Wang, S., Xiao, M., Han, D., Hickner, M.A., and Meng, Y. *RSC Adv***.**, 2013, **3**, 15467-15474. DOI: 10.1039/C3RA41670D

23 Drake, H.L., Kusel, K., and Matthies, C. *Prokaryotes*, 2006, **2**, 354-420. Accessed via http://bionumbers.hms.harvard.edu/bionumber.aspx?id=104403&ver=0.

24 “Fluorine-Doped Tin Oxide, FTO Glass.” Materials Safety Data Sheet: MTI Corporation, 2007.